OBSERVING THE EFFECTS OF THE SURF ZONE ON LOCAL SEA SALT AEROSOL PRODUCTION

A THESIS SUBMITTED TO THE UNDERGRADUATE DIVISION OF THE UNIVERSITY OF HAWAIʻI AT MĀNOA IN PARTIAL FULFILLMENT OF THE REQUIREMENTS FOR THE DEGREE OF

BACHELOR OF SCIENCE

IN

GEOLOGY AND GEOPHYSICS WITH A RESEARCH TRACK

May 2020

By

Katherine Ackerman

Thesis Advisor:

Dr. Alison Nugent

I certify that I have read this thesis and that, in my opinion, it is satisfactory in scope and quality.

THESIS ADVISOR

Dr. Alison Nugent, Department of Atmospheric Sciences

Acknowledgements

This material is based upon work supported by the National Science Foundation under EAGER Grant No. 1762166, and the Undergraduate Opportunities Program at the University of Hawai'i at Mānoa. Any opinions, findings, and conclusions or recommendations expressed in this material are those of the author and do not necessarily reflect the views of the National Science Foundation or the Undergraduate Opportunities Program.

I would like to thank Dr. Alison Nugent for her immense guidance, encouragement, and support. Dr. Nugent accepted me as an undergraduate with no background in atmospheric science and was extremely patient, helpful and supportive of all of my academic goals. I am grateful to have had her for my mentor for two years, as she's made me the scientist I am today.

I would also like to thank Aaron Taing. Aaron accompanied me on every sampling session in addition to providing mentorship, encouragement, and friendship throughout my academic journey. Additionally, he prepared much of the code used to analyze this data and has set up the lab with several well-written scripts for future analysis.

I am grateful for my SOEST advisors, Dr. Bridget Smith-Konter, Dr. Greg Ravizza, and Leona Anthony. All three of my advisors worked tirelessly with me to ensure my goals were possible, in addition to working with me to accommodate the oddities of my degree requirements.

Finally, I would like to thank my friends and family for supporting all of my goals. I would especially like to thank my sister Grace, Mom, Dad, and boyfriend Kelton for their encouragement. None of my accomplishments would have been possible without their love and support, and I am grateful to have had them as part of my academic journey.

ABSTRACT

Sea spray aerosols (SSA) play a significant role in the local climatology of coastal areas by acting as cloud condensation nuclei and through direct radiative forcing. Quantifying the size distribution and concentration of SSA is essential to understanding their influence in coastal regions. However, there has been no quantification of how SSA production changes from open ocean to the coast. With the advent of the Giant Nucleus Impactor (GNI) from NCAR, greater information can be obtained about SSA sizes and concentrations. A smaller, low-cost instrument known as the mini-GNI was created by modifying the NCAR GNI at the University of Hawai‘i at Mānoa, making SSA sampling at specific locations and altitudes highly accessible. Using a drone, the mini-GNI was used to sample four locations over the ocean perpendicular to the coastline: the open-ocean, fringing reef, lagoon, and shoreline. A quantitative understanding of how SSA sizes and concentrations change as ocean winds approach the coastline can be developed using open ocean concentrations as a baseline concentration. Overall, a doubling of SSA concentrations and total mass was observed from open-ocean concentrations to the shoreline, and the highest SSA production was observed with offshore waves passing over the fringing reef crest.

Table of Contents

List of Figures

Figure 7. This diagram displays the sampling methodology with respect to height or depth (in meters) and distance from the shore (in 10s of meters). Bathymetry (cyan), average sea level height (blue), and drone height (orange) are displayed, along with the ranges of sampling from the shore (black), lagoon (yellow), reef (teal), and ocean (red) regions.

Figure 8. This is a sample image from one of the 350 images taken by the optical microscope of each polycarbonate slide. The two arrows point towards flatter droplets with reduced surface tension, possibly due to organic material, resulting in their lighter coloring. All others are assumed to be cap drops grown on SSA. Figure 4 from Jensen et al. (2020a).

Figure 9. This plot shows how the (left) number concentration of SSA (m^{-3}) and (right) Total SSA Mass (m^{-3}) changed with distance from the shore (m) on three sample days: (top) 190930, (middle) 191004, and (bottom) 200227. A value of 800 m on the x-axis represents open-ocean concentrations, while any distance <600 m represents samples within the surf zone. Each sample point indicates a different SSA sample slide, sample point color indicates wave height (m), and size indicates surface wind speed (m/s). A line of best fit (red) is given, along with its equation and correlation.

Figure 10. The total number concentration (left, m^{-3}) and total mass concentration (right, $\mu g/m^3$) are plotted against distance from the shore (m) for 190906 (top) and 200227 (bottom). Each scatter point is sized by surface wind speed (m) and colored by significant wave height (m).

Figure 11. The normalized number concentration (left) and normalized total mass concentration (right) are plotted against distance from shore (m) for all samples. Each scatter point is sized by wind speed (m/s) and colored by significant wave height (m). Encircled are areas of strong (blue) and weak (red) correlation between normalized concentration and distance from shore.

Figure 12. The total number concentration (left, m^{-3}) and total mass concentration (right, $\mu g/m^3$) are plotted against surface wind speed (m/s). Each scatter point is sized by the significant wave height (m) and colored by the total distance from the shore (m).

Figure 13. The cumulative number concentration (m^{-3}) of SSA on a log scale is plotted against the dry radius bins (μm) of the size distribution. Each line represents a different sample and is colored by the mean wind speed (m/s) of the sample.

Figure 14. The total number concentration (left, m^{-3}) and total mass concentration (right, $\mu g/m^3$) are plotted against surface wind speed (m/s) for ocean (top), reef (middle), and lagoon (bottom) samples. Each scatter point is sized by the significant wave height (m) and colored by the total distance from the shore (m).

Figure 15. An example image of the PacIOOS model. The significant wave height (m) is represented by color. The circled black region represents the two grid points used for significant wave height.

Figure 16. The total number concentrations (m^{-3}) are plotted against significant wave height (m) for four sampling days; 190906 (top left), 190930 (top right), 191004 (bottom left), and 200227 (bottom right). Each scatter point is sized by the surface wind speed (m/s) and colored by the total distance from the shore (m).

List of Abbreviations

Abbreviation	Definition
SSA	Sea Salt Aerosol
MBL	Marine Boundary Layer
RH	Relative Humidity
CCN	Cloud Condensation Nuclei
MSE	Mass Scattering Efficiency
GCCN	Giant Cloud Condensation Nuclei
VAMOS	Variability of the American Monsoon Systems
VOCALS	VAMOS-Ocean-Cloud-Atmoshpere-Land Study
FSSP	Forward Scattering Spectrometer Probes
mini-GNI	Miniature Giant Nucleus Impactor
NCAR	National Center for Atmospheric Research
K5500	Kestrel 5500 Weather Meter
CE	Collision Efficiency
PacIOOS	Pacific Islands Ocean Observation System

Symbol	
r_{80}	Radius at 80% relative humidity
r_d	Radius at 0% relative humidity

Chapter 1: Introduction

1.1 Background

Sea spray aerosols (SSA) are natural aerosols produced by waves breaking on the sea surface. SSA consist primarily of sodium chloride and are the largest naturally produced aerosol by mass in the world. Their highly hygroscopic nature makes them an important aerosol in the marine boundary layer (MBL) as they readily act as cloud condensation nuclei, influencing cloud formation and precipitation rates (Lewis and Schwartz, 2004). Because of their physical abundance, it is important to accurately quantify their presence in the atmosphere in order to understand their potential influence.

It is important to define the size convention of SSA within this study to prevent any ambiguity. Discussions of SSA often define size by r80, or the equilibrium radius at 80% relative humidity (RH), where r80 is two times the radius of the dry aerosol mass (Lewis and Schwartz, 2004). SSA size in this study is defined in their dry radius, or r_d, unless otherwise specified. Additionally, while SSA can exist as accumulation (r_d <0.5 um) and coarse mode (r_d >0.5 um) aerosols, this experiment strictly analyzes coarse model SSA.

1.2 Production and Flux of Sea Salt Aerosols

SSA are categorized by the method in which they are produced on the ocean surface. The first and most abundant method of production is the entrainment of air into bubbles by breaking waves These bubbles eventually pop, releasing 10s to 100s of tiny sea water drops known as film drops, which are the smallest ($0.05 < r_d < 2.5$ μm) SSA produced (Lewis and Schwartz, 2004). After the film bursts, the resulting bubble crater is rapidly filled with water, resulting in the ejection of a vertical jet of water. The high acceleration upward releases an additional 1 to 10 drops known as jet drops ($2.5 < r_d < 12.5$ μm) (Lewis and Schwartz, 2004). The last and largest

SSA produced occur when wind speeds exceed 9 m/s. The high winds physically shear seawater droplets known as spume drops (r_d > 12.5 µm) from the surface of breaking waves (Anguelova, 2002).

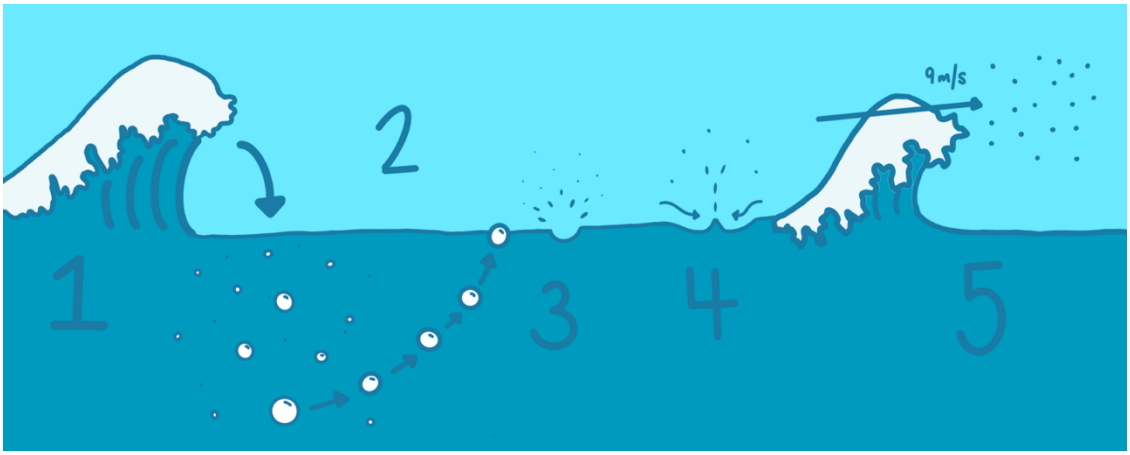

Figure 1. These are the stages and methods in which SSA are produced. Position 1 represents waves breaking or ocean white caps. This entrains air into the water represented by position 2. As the bubbles rise towards the surface, they pop releasing up to hundreds of film-drops at position 3. The popping of the bubble surface causes the bubble crater to collapse in on itself, represented by position 4, which then shoots a jet of water into the air producing jet droplets. The final method is dependent on wind speeds over 9 m/s and produces spume droplets when the shear force of the wind tears large droplets from the crests of breaking waves.

The atmospheric residence times of SSA depends on size. Small SSA particles (0.1 < r_d < 1 µm), which are believed to readily mix vertically within the marine boundary layer (Lewis and Schwartz, 2004). Because of their relatively small mass, gravitational fallout is negligible, making wet deposition, or deposition through precipitation, the predominant form of removal for small SSA (Lewis and Schwartz, 2004). This implies that they can remain suspended for weeks if rain is absent and therefore have the highest likelihood of accumulating in large concentrations (Lewis and Schwartz, 2004).

Medium-sized SSA particles (0.5 < r_d < 12 µm) have a larger mass than small SSA particles, causing gravitational fallout to be the predominant method of removal, and the average

atmospheric residence of these particles' ranges from days to only minutes (Lewis and Schwartz, 2004).

The largest SSA (r_d > 12 μm) often have atmospheric residence times of only seconds. Their large mass makes it difficult for them to enter the atmosphere beyond a few meters of their production sites (Lewis and Schwartz, 2004).

Because the nature of SSA production appears to rely predominantly on surface winds, many model source functions prioritize instantaneous wind speed as the dominant variable in SSA production. However, in a coastal environment, these production mechanisms can be accelerated. Changes in bathymetry can drive an increase in breaking waves, accelerating the production of film and jet drops (Anguelova, 2002).

1.3 Significance of Sea Salt Aerosols

SSA can influence atmospheric conditions through direct and indirect radiative forcing, through chemical reactions in the troposphere, and by acting as cloud condensation nuclei (CCN). While most direct radiative forcing comes from accumulation mode SSA, not the focus of this study, accumulation mode concentrations are expected to increase in the surf zone due to a general increase in SSA production.

SSA can have a high affinity for scattering solar radiation in the MBL, with regions dominated by SSA showing single-scattering albedo as high as 0.97 (Hsu, 2019). In coastal communities, an estimated 52% of total light extinction can come from local SSA production (Lowenthal & Kumar, 2012). This scattering efficiency is not only important for radiation budgets in climate models for marine and coastal regions, but also proves significant where the U.S. Environmental Protection Agency's Regional Haze Rule utilizes light scattering extinction as a means of assessing air pollution levels (Lowenthal & Kumar, 2012). A clear

relationship between the relative radius of SSA and their mass scattering efficiency is demonstrated by Figure 2 (McInnes, Bergin, Ogren, & Schwartz, 1998). Accurate representation of SSA is important for understanding the underlying scattering effects contributed by SSA in the global radiative budget.

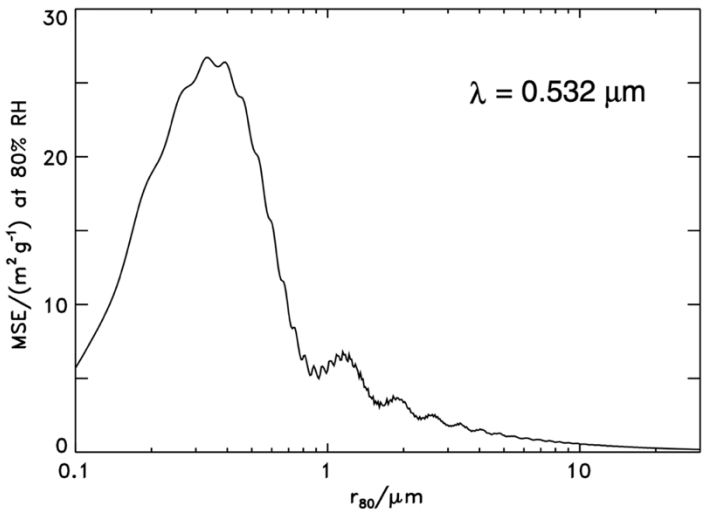

Figure 2. By McInnes et al., 1998. A relationship between the radius of SSA at r_{80} and the mass scattering efficiency (MSE) per area by mass at the given wavelength 0.532 μm. This relationship depends strongly on SSA radius, and therefore quantifying the potential MSE/m^2 depends strongly on accurately representing the concentrations of varying SSA radii.

Additionally, SSA can indirectly influence short-wave radiation through their ability to act as CCN. The highly hygroscopic nature of SSA makes them excellent CCN and their concentrations determine their indirect radiative potential. As the Twomey Effect describes, the concentrations of these CCN may influence the amount of solar radiation reflected by clouds. It is hypothesized that increasing (decreasing) the concentration of aerosols present in an air parcel with fixed liquid water content will result in more (fewer) cloud droplets with smaller (larger) radii, therefore increasing (decreasing) the overall albedo of the cloud (Twomey, 1974).

In addition to scattering potential, coarse mode SSA (r_d > 0.5 microns) can act as giant CCN (GCCN) which are hypothesized to accelerate warm rain initiation (Jensen and Nugent, 2017). A study by Jensen and Nugent (2017) demonstrates that GCCN with r_d > 2 μm remain as concentrated salt solutions, aiding in accelerating their condensational growth in comparison to pure liquid water droplets during adiabatic lifting. In regions like the Hawaiian Islands, quantifying and identifying variables that contribute to accelerated production and vertical lifting of GCCN to cloud base will aid in understanding the initiation of warm precipitation on the windward coasts of the islands.

1.4 Current In-Situ Observations

Several sampling methods have attempted to observe SSA over the last 70 years. A widely used method involves attaching a cascade impactor equipped with different cone-shaped inlet nozzles to the side of a ship or aircraft. The impactor collects information on cumulative SSA mass at different cutoff radii, and it has been used in both the Variability of the American Monsoon Systems (VAMOS) Ocean- Cloud- Atmosphere- Land Study (VOCALS) in 2008 and the Asian Pacific Regional Aerosol Characterization Experiment (ACE-Asia) in 2001 for both aircraft and ship measurements (Jaeglé, 2011). The cascade impactor method provides information on the total mass of aerosols of different sizes. However, aerosol concentrations are not directly observed using this method.

Another method for observing SSA involves the Forward Scattering Spectrometer Probes (FSSP), which obtains the size and concentration of aerosols passing through it. A downfall of the FSSP method is that it was originally designed to observe cloud droplets, and it is therefore unable to distinguish between pure droplets or deliquesced SSA (Lasher-Trapp and Stachnik, 2007).

The third and oldest method used to observe SSA is the external impactor method. This method, first developed by Dr. Alfred Woodcock in the 1950s, involves mounting glass slides coated with an oily film onto aircraft (Woodcock, 1952). Over the duration of a flight, water droplets impact onto the slide, leaving hemispheric impressions. These slides are then placed in a chamber with controlled temperature and humidity overnight for the SSA to reach equilibrium size within the chamber environment. In the morning the slides are then analyzed by an optical microscope for SSA size and concentrations, allowing for the observation of SSA size distribution.

Most field campaigns have been conducted to observe SSA over the open-ocean, and much fewer studies have been attempted to study SSA production in the surf zone. The University of Miami has attempted to characterize surf zone production using over 35 coastal stations that monitor major aerosol species like SSA through high-volume filter samplers. The filter is analyzed by ion chromatography to find the sodium and chloride ion mass present (Jaégle, 2011), so while mass is retained, information on the SSA size distribution is lost.

1.5 Study Objectives

Given the importance of SSA to coastal communities, and the strong probability that coastal conditions aid in SSA production, the objectives of this experiment are to observe SSA concentrations across the surf zone, quantify the changes in SSA concentrations between the open ocean and the surf zone, and to relate the concentration differences observed to changes in coastal variables. Sampling is performed using a drone and new sampling instrumentation known as the miniature Giant Nucleus Impactor, or mini-GNI, at four discrete locations perpendicular to the shoreline of Lanikai Beach on this island of O‘ahu.

Chapter 2: Methodology

2.1 Instrumentation

2.1.1 Drone

The drone offers the ability to sample SSA concentrations at various distances from the coast, providing insight into how environmental conditions affect SSA concentrations as they approach the shoreline. A Yuneec Typhoon H-Hexacopter drone was chosen for the increased flight stability and lift capacity needed to carry two mini-GNI instruments for sampling SSA. The camera on the drone provided a video record of wave conditions at each sampling location in addition to a view of the instruments. This helped to confirm that the instruments were opening and closing at the precise sampling locations. Once at each sampling location, the drone remains in a stationary hover for the duration of sampling at an average altitude of 12 meters. The altitude was confirmed with the drone's built-in barometer. Maintaining consistency in the sampling altitudes is important to understanding how SSA concentrations change with distance from the shoreline rather than with height. Additionally, the drone GPS provided the latitude and longitude of each sample taken, along with the total distance from shore, which were manually recorded during sampling.

2.1.2 Mini-GNI

The miniature Giant Nucleus Impactor, or mini-GNI, was developed after the GNI from the National Center for Atmospheric Research (NCAR). It functions by exposing a polycarbonate slide to the free airstream, allowing deliquesced salt particles to impact onto it. In the mini-GNI, the polycarbonate slide is located within a small 3-D printed housing device consisting of a base, a door, and a mechanical arm to hold the polycarbonate slide. When the mini-GNI is not sampling, the door remains closed, protecting the slide from unwanted exposure

to SSA. This allows precise sampling in time and location. The base of the mini-GNI is equipped with a hollow wing wrapped in plastic wrap to allow the instrument to orient itself parallel to the wind direction. Because the slide is perpendicular to the wing, this helps to maximize the collision efficiency of SSA on the slide.

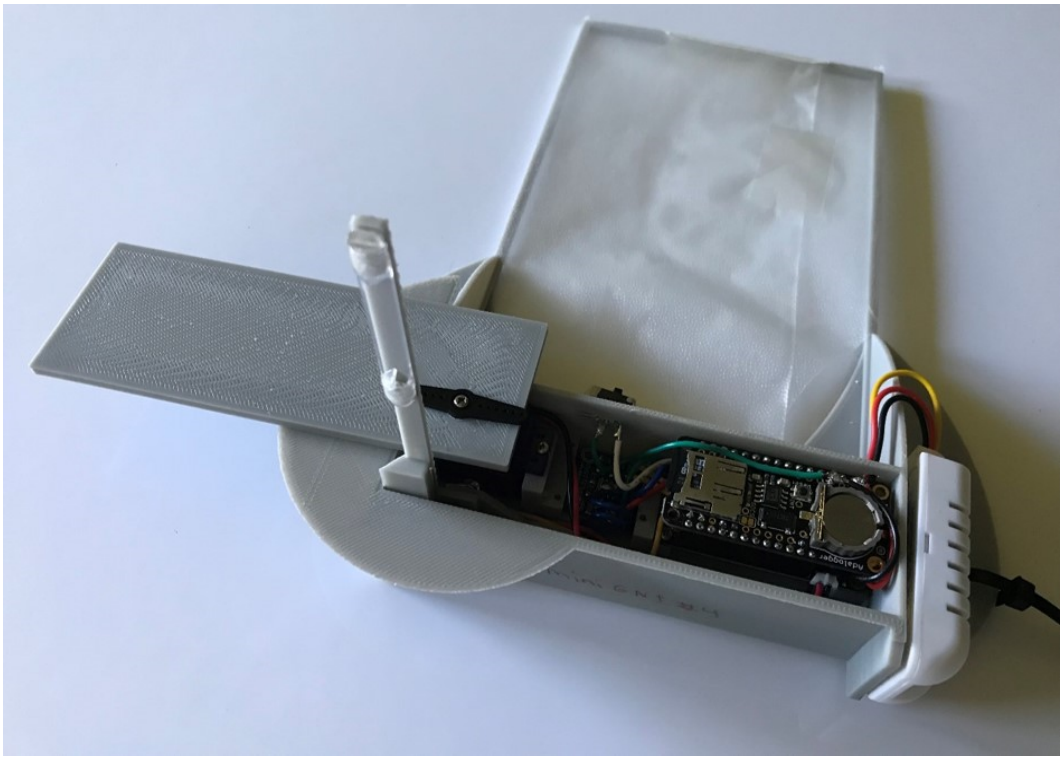

Figure 3. A picture of the mini-GNI instrument used for sampling SSA. In this particular photograph, the door of the instrument is open, showing the instrument's arm with a polycarbonate slide attached. The Arduino microcontroller inside the body of the instrument is also visible.

The mini-GNI also houses sensors that measure temperature, relative humidity, and pressure. The data is stored in a text file on a micro-SD card add-on and can be easily uploaded to a computer for analysis.

During sampling, two mini-GNIs hung freely beneath the drone at a length of five and seven meters, respectively. The length was required to ensure that air displaced from the drone's propellers would not interfere with the airstream impacting the polycarbonate slide, and that air

displaced from one mini-GNI would not interfere with the other. Two mini-GNIs were used to increase the sample size and to ensure a sample was taken in case one mini-GNI failed.

2.1.3 Kestrel

In order to measure environmental conditions while sampling, a Kestrel 5500 Weather Meter (K5500) was mounted on a tripod on the beach just above the high-tide line to measure surface winds, wind direction, temperature, and relative humidity. The kestrel measures surface winds using an anemometer with an accuracy of 0.1 m/s (Kestrel 5 Series Weather/Environmental Meters, 2020). The measured surface wind is later used to calculate the sample volume and collision efficiency.

2.2 Location

2.2.1 Bathymetry

Sampling occurred along the eastern coast of O`ahu at the northern portion of Lanikai Beach (Figure 4). This beach was chosen for its bathymetry and orientation perpendicular to the trade winds. It exists on a long stretch of the eastern O`ahu shelf and the bathymetry changes less than 200 m over 10 km as the ocean floor approaches the shore. Within the last kilometer before the shore, a large fringing reef is present. This reef produces consistent wave breaking even under wave heights as minimal as 1-2 feet and is therefore a potential source for consistent SSA production. Between the reef crest and shore exists a shallow lagoon that exhibits minimal wave breaking from the combination of the attenuation provided by the outer reef crest and the minimal changes in bathymetry. This lagoon area provides a region in which presumably minimal SSA production is occurring, and there is hypothesized to be a net loss in SSA concentration as the largest particles produced by the reef crest are removed by dry deposition.

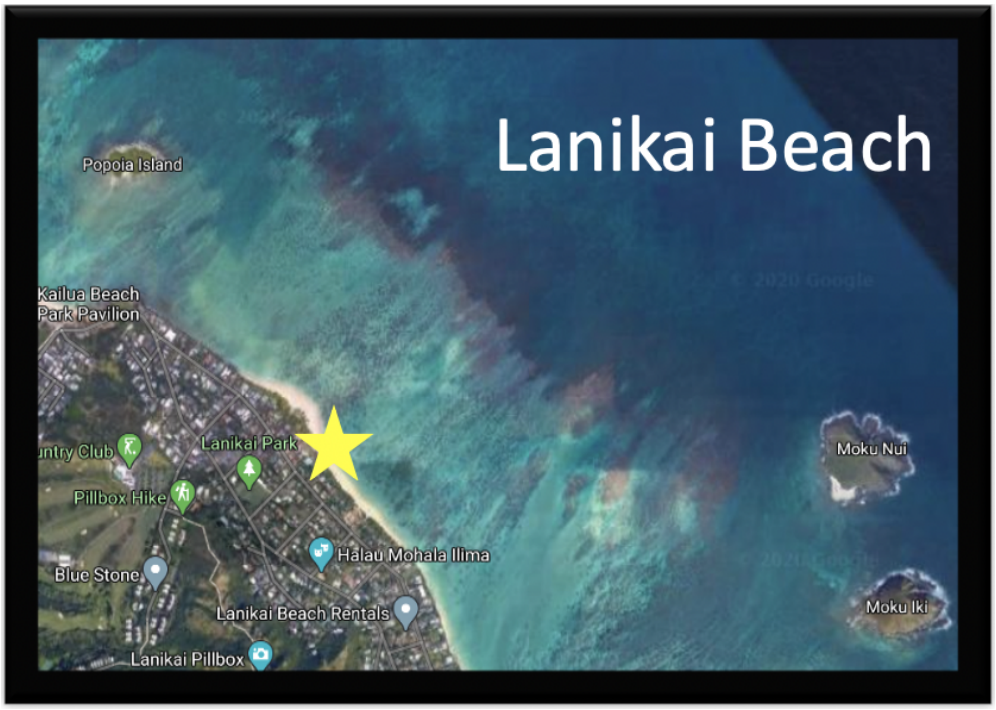

Figure 4. A satellite image showing the region offshore of Lanikai beach where sampling takes place. A fringe reef is clearly visible in the image, and a star denotes the location where the Kestrel is placed on the shoreline.

2.2.2 Trade Winds

Lanikai beach has an average strike of 135 degrees southeast, proving to be almost exactly perpendicular to the average direction of the Northeast Trade Winds (between 22.5 and 62.5 degrees) (Garza et al., 2012). The offshore waves produced on the eastern portion of the island are generally Northeast trade waves from 0-123 degrees; the result of fetch produced by the trade winds (Garza, Chu, Norton, & Schroeder, 2012). By sampling in a region with similar wave and wind orientation as well as a coastline that is perpendicular to both wind and waves, the SSA samples are ensured to have interacted with offshore waves and winds in the same general direction. The position of Lanikai perpendicular to the waves and wind is strategic for maintaining this consistency, as nearshore waves will always orient themselves perpendicular to the shoreline while wind direction is independent of this. Lanikai beach maintains winds and

waves with similar origination orientation, therefore ensuring that the aerosols present in the sample originate and interact within the same flume of air and ocean waves.

2.2.3 Significant Wave Height

In order to understand how bathymetry changes in the surf zone contribute to the significant wave height of waves approaching the coast, the Pacific Islands Ocean Observation System (PacIOOS) coastal wave model is used for analysis. The PacIOOS wave model utilizes significant wave height from the Mokapu buoy, located off of the coast of Lanikai beach. Every hour, the wave model takes the peak significant wave height and resolves a new significant wave height for a 500 m by 500 m grid square. The modeled significant wave height was then used in analysis.

2.3 Sampling Locations

Using the drone, sampling with the mini-GNIs occurred at four separate locations; the open-ocean, fringing reef, lagoon, and shoreline (Figure 5). Sampling at four distinct locations gives greater insight into how SSA concentrations change from the open ocean to the shoreline and has the potential to identify regions where production is the highest. This allows us to assess each sampling location individually for specific changes in the environment, which may demonstrate how coastal and environmental variables affect SSA production and concentration changes.

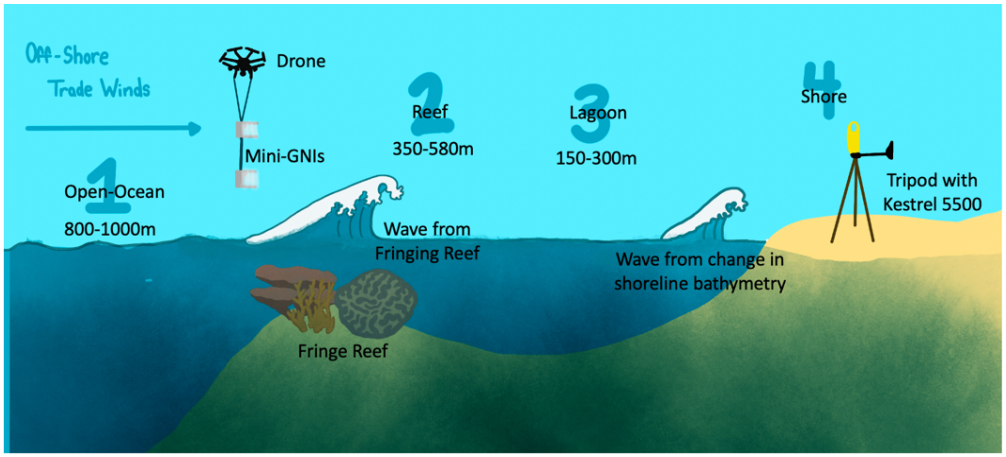

Figure 5. A cartoon schematic of the sampling methodology. As the trade winds move onshore (left to right as viewed from the North), SSA is sampled with two mini-GNIs attached to a drone at four locations: (1) open ocean 800-1,000 m offshore, (2) reef 350-580 m offshore, (3) lagoon 150-300 m offshore, and (4) shore. Meanwhile the kestrel measures wind speed from a tripod on the shore.

Because SSA have residence times ranging from hours to weeks, measuring an open-ocean sample is essential to establishing a background concentration to compare against the three other sampling locations. The open-ocean sampling occurs between 800-1000m off of the coastline, shown in red in Figure 6.

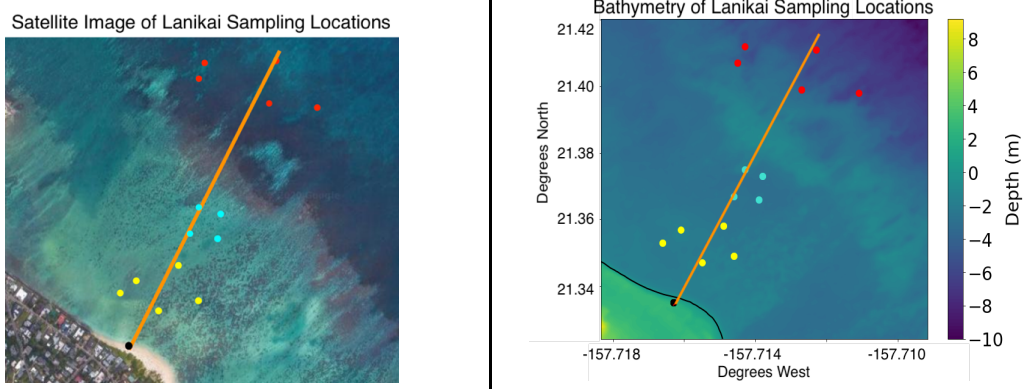

Figure 6. All mini-GNI SSA samples analyzed in the present study are shown (left) on a satellite image, and (right) over bathymetry for the region offshore of Lanikai beach. The orange lines show the average drone path, perpendicular to the shore and the color of the samples coincides with Figure 7 designating ocean (red), reef (teal), lagoon (yellow), or shore (black).

The distance offshore for this sample was initially chosen using the drone's camera to determine where white-capping diminished. Plotting the latitude and longitude coordinates from the drone also verified that the open ocean samples were beyond the most distinguishable nearshore bathymetric feature, the fringing reef. The range of open-ocean sampling distances is indicated by the red shaded area in Figure 7.

Within the same sampling day, samples were taken within either the Reef or Lagoon locations, or both, maintaining the same altitude of the ocean samples. The Reef sampling location exists between 350-500 m offshore (teal shading in Figure 7), positioned directly onshore of the prominent fringing reef. As offshore waves begin to interact with the bathymetry, potential energy within the wave is converted into kinetic energy, and the wave begins to steepen. Once the waves reach the outer reef, they often crest, producing visible whitecaps. Using the drone's camera, the Reef location was chosen based on the increased whitecap coverage in this area and the visible fringing reef at this location, and then validated using the GPS data.

The Lagoon and Shore sampling locations were then taken as measurements intended to represent a region of calmer waves. Lagoon samples were between 150-300 m offshore (yellow shading in Figure 7), while the Shore samples are at location "0" for the purpose of this experiment (black line in Figure 7). It is important to note that the shore samples were only taken on one sampling day, and therefore the analysis of their concentrations against changes in coastal conditions is minimal, given the small range of change in many of the coastal conditions within that sampling day.

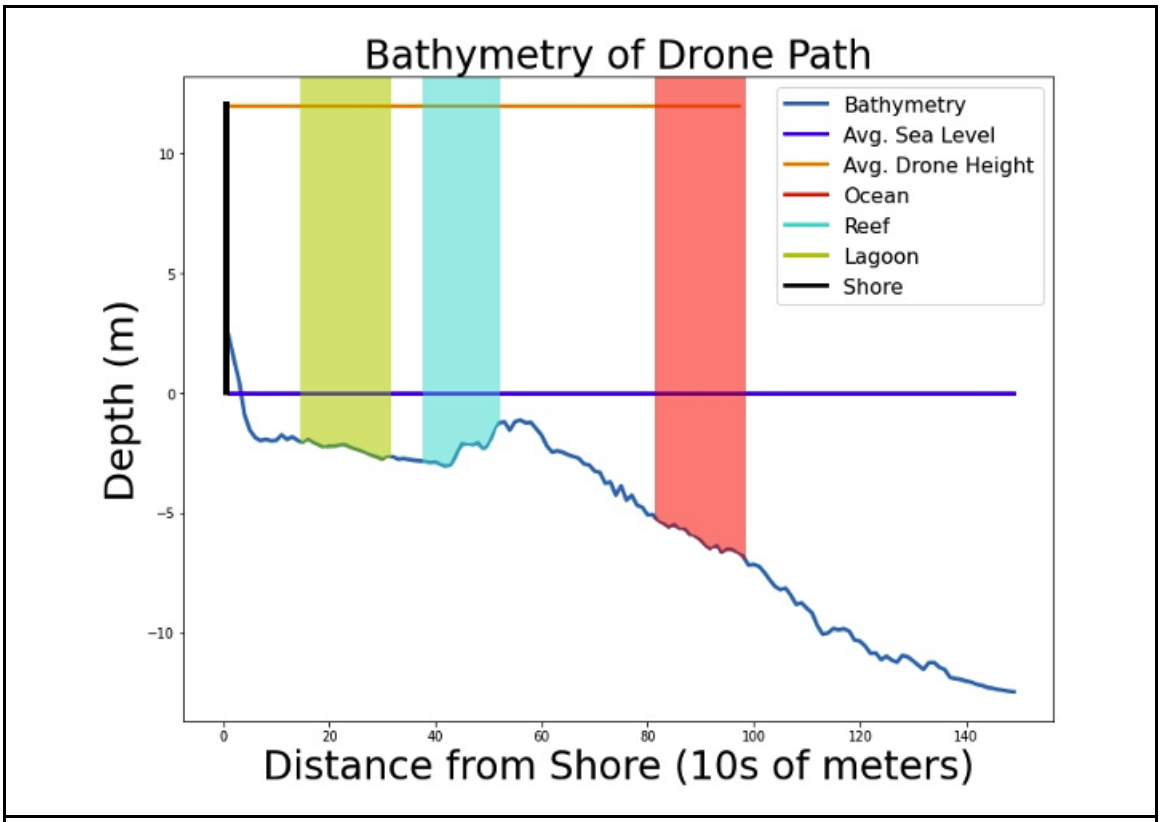

Figure 7. This diagram displays the sampling methodology with respect to height or depth (in meters) and distance from the shore (in 10s of meters). Bathymetry (cyan), average sea level height (blue), and drone height (orange) are displayed, along with the ranges of sampling from the shore (black), lagoon (yellow), reef (teal), and ocean (red) regions.

2.4 Wind Speed Aloft

Because SSA sampling occurred 10 meters above the wind sampling, wind speed aloft needs to be considered. Using known relationships between surface wind speeds and wind speeds aloft, the power law (EQ. 1) and the log law (EQ. 2) were used to estimate wind speed at the height of SSA sampling:

$$EQ.1 \qquad v_2 = v_1 * (\frac{z_2}{z_1})^{\alpha} \qquad\qquad EQ.2 \qquad v_2 = v_1 * \frac{ln\left(\frac{z_2}{z_0}\right)}{ln\left(\frac{z_1}{z_0}\right)}$$

where v_1 is the measured wind speed at altitude z_1, v_2 is the calculated wind speed at altitude z_2, z_0 is a term representing surface roughness, and α is a term representing the stability of the

atmosphere. Because sampling heights and surface roughness remained constant across the sampling days, the calculated wind speeds aloft were 1.17x greater and 1.31x greater than the 2-meter wind speeds for the power law and log law respectively. The increase in magnitude did not affect the r-squared correlation between wind speeds and concentrations and total mass. Therefore, only surface winds are used hereafter.

2.5 Slide Analysis

Once the polycarbonate slides are collected from the mini-GNIs after sampling, they are placed into small tubes filled with desiccant to dehydrate any liquid water present. These tubes are sent in batches to NCAR for analysis using the GNI microscope, where the slides are placed inside a humidified chamber at 33.5°C and 90% relative humidity (Jensen 2020a). Because SSA are extremely hygroscopic, they form spherical caps when humidified which helps to distinguish them from other types of particles that may also impact onto the slide. Once the slide reaches equilibrium, an automated optical microscope captures 350 images of every single polycarbonate slide, similar to the image shown in Figure 8, which are then analyzed by a computer. Software counts and sorts each droplet imaged by the optical microscope by radius from 1-25 μm with bin sizes of 0.2 μm (Jensen, 2020a).

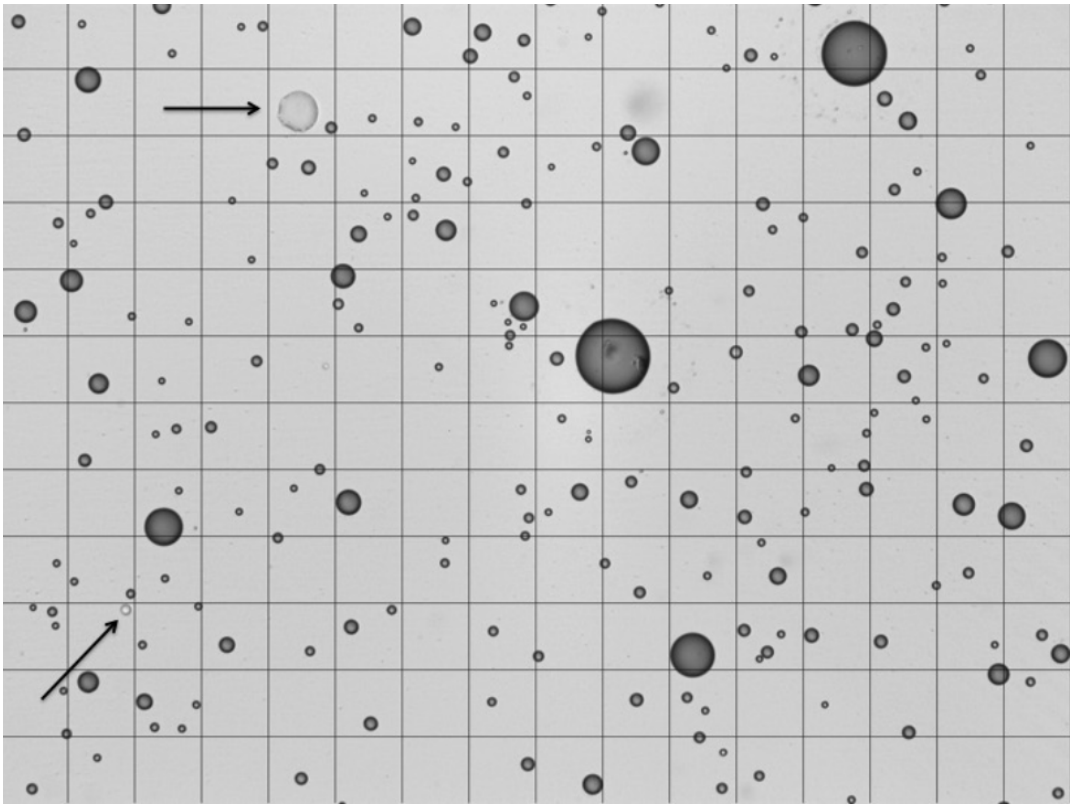

Figure 8. This is a sample image from one of the 350 images taken by the optical microscope of each polycarbonate slide. The two arrows point towards flatter droplets with reduced surface tension, possibly due to organic material, resulting in their lighter coloring. All others are assumed to be cap drops grown on SSA. Figure 4 from Jensen et al. (2020a).

Once completed, the software program then calculates the total number concentration of SSA (N_{SSA}) by using the raw count of SSA present on the side (N_{raw}) and dividing it by the total sample volume (V_S) multiplied by the collision efficiency (CE) of SSA particles impacting the slide:

$$N_{SSA} = \frac{N_{raw}}{V_S \cdot CE} \quad \text{EQ. 3}$$

The total sample volume is calculated using the area of the slide multiplied by the sample duration and wind speed. The CE is used to represent the fraction of SSA particles that are

impacted onto the slide instead of following the airstream around it. Because different sized SSA have different masses, larger SSA have a higher CE than smaller SSA. A cutoff radius for analysis was determined by setting a cutoff collision efficiency of 40%.

Chapter 3: Results and Discussion

Of the 51 slides collected over 8 separate sampling sessions, only 30 slides across 4 days were used in this analysis. Given the novelty of this sampling methodology, the sampling duration for many of the first slides were too short resulting in small loading, or small SSA concentrations on the slides. Because of this, the microscope was unable to analyze 21 of the 51 samples.

3.1 Distance from Shore

The primary goal of this research was to determine whether SSA concentrations and mass change with distance across the surf zone. Figure 9 shows the relationship between SSA number concentration and total salt mass with distance from the shore from three sample days: 190930, 191004, and 200227 (YYMMDD format). While the magnitudes vary each day, there is a strong correlation (r^2>0.83) between SSA number and mass with distance on all three sample days showing that total SSA concentrations and total SSA mass have a strong negative relationship with distance from shore.

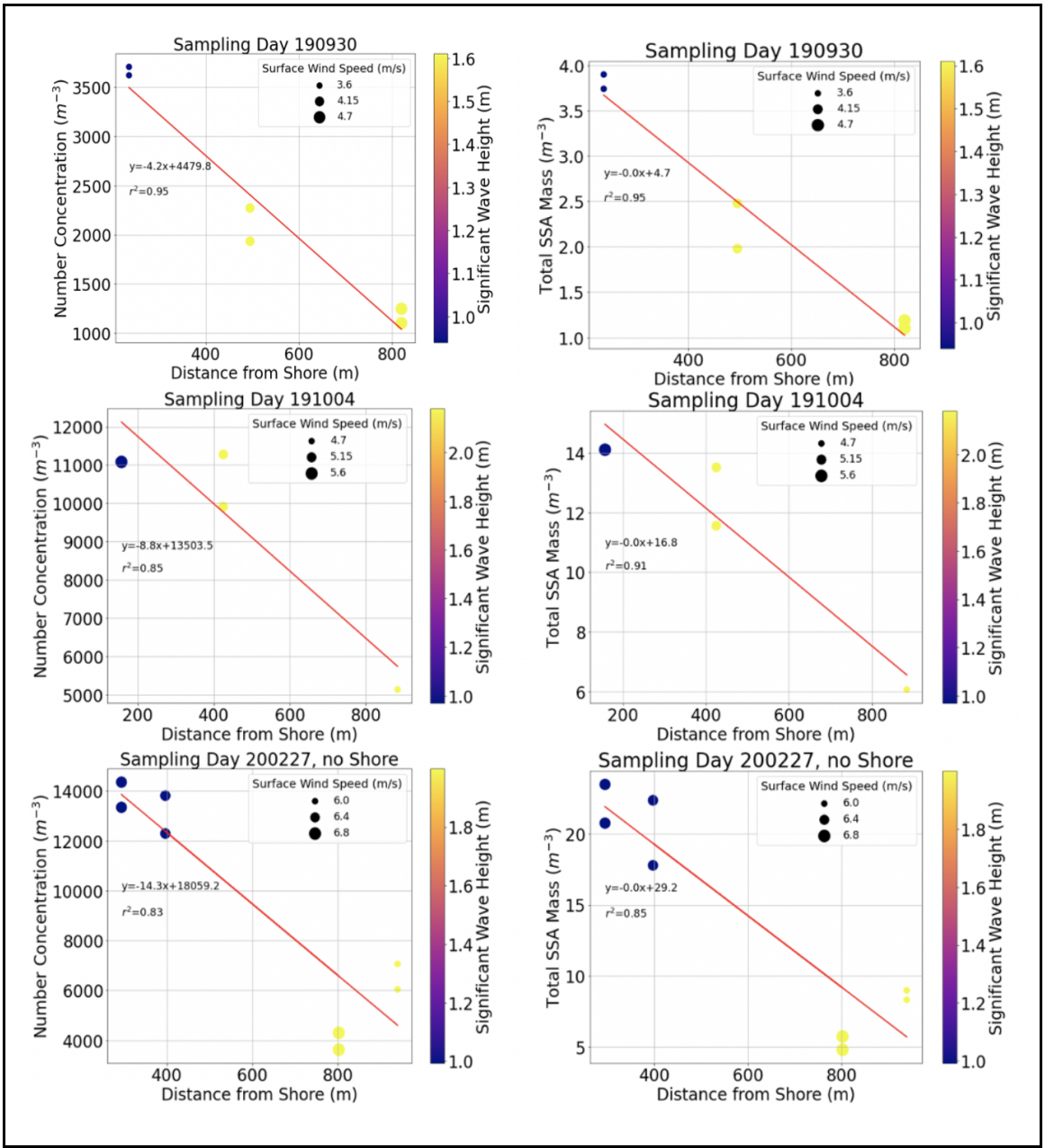

Figure 9. This plot shows how the (left) number concentration of SSA (m^{-3}) and (right) total SSA mass (m^{-3}) changed with distance from the shore (m) on three sample days: (top) 190930, (middle) 191004, and (bottom) 200227. On the x-axis, a value of 800 m represents open-ocean concentrations, while any distance <600 m represents samples within the surf zone. Each sample point indicates a different SSA sample slide, color indicates wave height (m), and size indicates surface wind speed (m/s). A line of best fit (red) is given, along with its equation and r^2 value.

A strong relationship between number concentration or total SSA mass and distance from shore was not found on all sampling days. For example, 190906 as well as 200227 when the shore samples are included, show more complicated relationships (Figure 10).

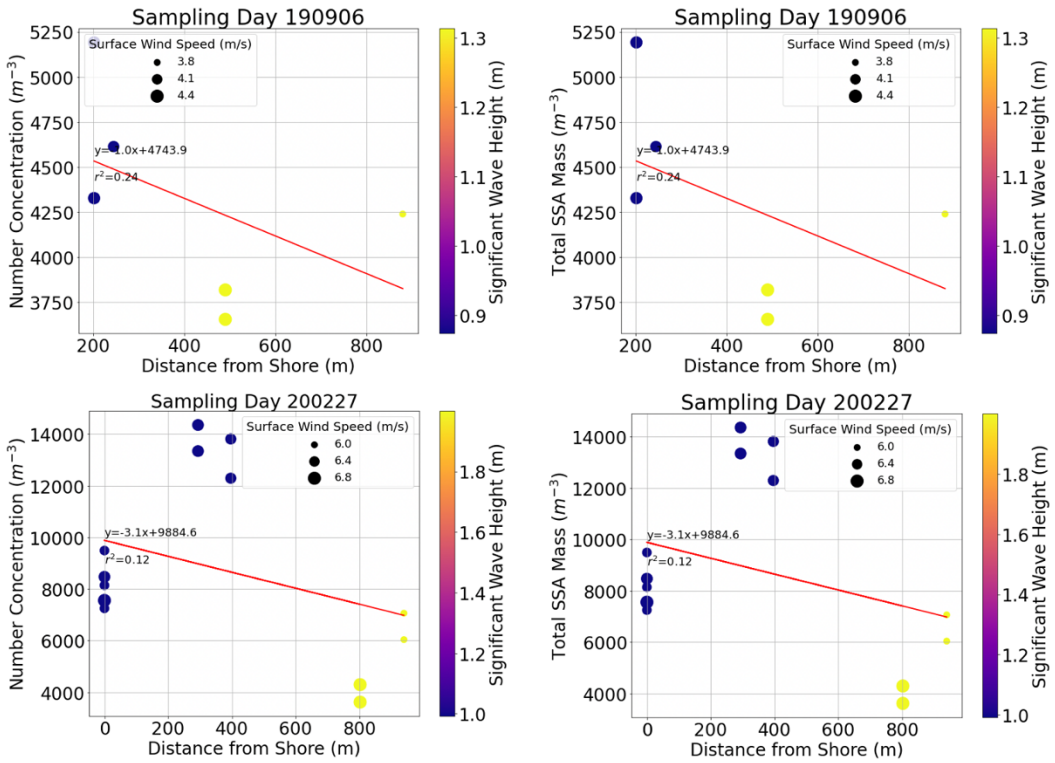

Figure 10. The total number concentration (left, m^{-3}) and total mass concentration (right, $\mu g/m^3$) are plotted against distance from the shore (m) for 190906 (top) and 200227 (bottom). Each scatter point is sized by surface wind speed (m) and colored by significant wave height (m).

Both 190906 and 200227 (Figure 10) have much smaller correlations between SSA number and mass with distance than the other sample days in Figure 9. On 190906, an increase in concentration from the open ocean to the lagoon was observed followed by a decrease in concentration from open ocean to the reef. On 200227, when including the shore samples, an increase from the open ocean concentrations to the reef was observed, followed by a decrease in

concentration from the reef to the shoreline. This is worth further investigation, as none of our current sampling techniques can offer an explanation for these anomalies.

Next, the concentrations were normalized against the open ocean concentrations, which are considered background SSA concentrations. Normalization uses equations 4 and 5 to understand the magnitude of change across the shoreline.

$$Normalized\ Concentration = \frac{Location\ Conc. - Open\ Ocean\ Conc.}{Open\ Ocean\ Conc.}$$

$$Normalized\ Mass = \frac{Location\ Mass - Open\ Ocean\ Mass}{Open\ Ocean\ Mass} \quad \text{EQ. 4, 5}$$

The normalized concentrations and masses show that most concentrations increase from their background concentrations toward shore, with over half of the samples exceeding background concentrations by at least 50% (Figure 11). Two samples nearly triple from the background concentration, and many samples at least double. For normalized mass, two samples more than triple, and many at least double.

Further analysis shows that the samples that occurred on days with strong correlations with distance to shore also show this same relationship when normalized (circled in blue, Figure 11). When weaker correlations with distance to shore were found, a weak relationship is still found after normalizing (circled in red, Figure 11). The size and color of the data points in Figure 11 denote wind speed and wave height, respectively, but no obvious pattern emerges suggesting that continued investigation is necessary for determining the SSA relationship with wind and wave height.

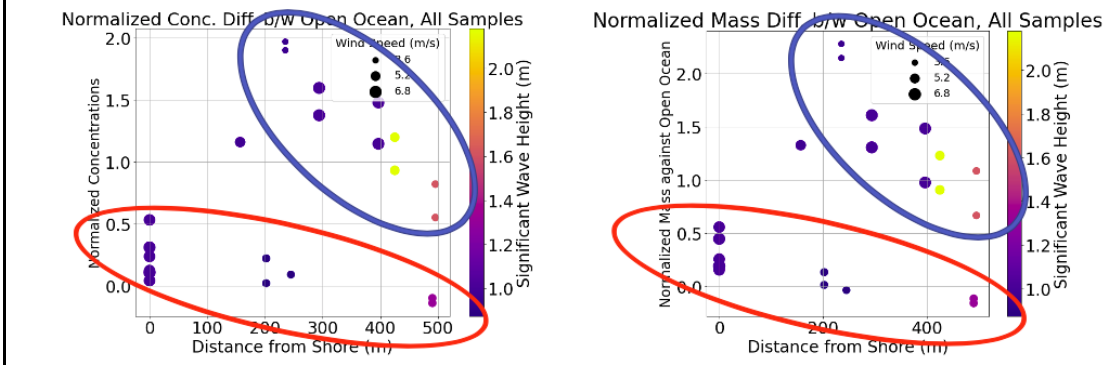

Figure 11. The normalized number concentration (left) and normalized total mass concentration (right) are plotted against distance from shore (m) for all samples. Each scatter point is sized by wind speed (m/s) and colored by significant wave height (m). Encircled are areas of strong (blue) and weak (red) correlation between normalized concentration and distance from shore.

3.2 Wind Speed

Instantaneous wind speed at 10 meters, or U_{10}, has generally been regarded as the most significant variable in SSA production over the open ocean (Grythe et. al, 2013). Overall, wind speed appears to account for 40% of total concentration variance, and 47% of total mass variance produced in the surf zone as shown by Figure 12.

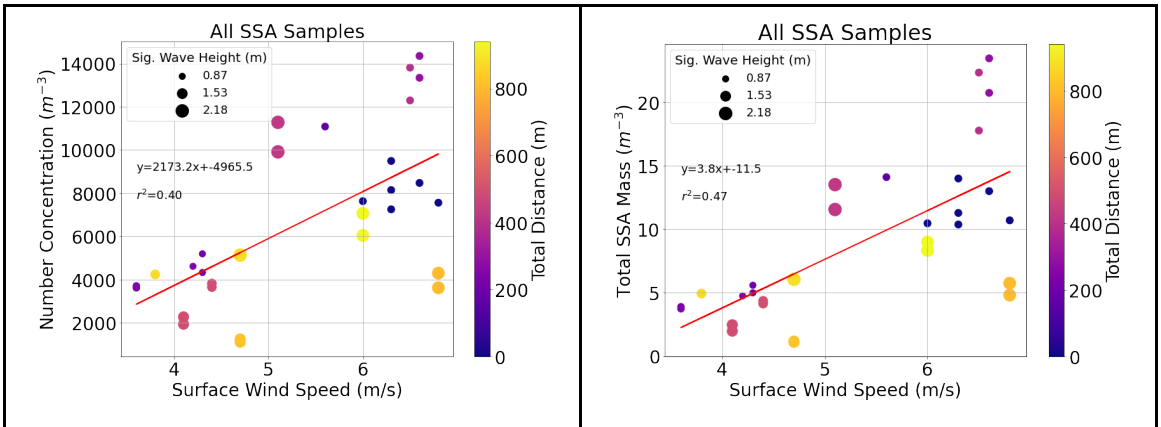

Figure 12. The total number concentration (left, m^{-3}) and total mass concentration

(right, µg/m^3) are plotted against surface wind speed (m/s). Each scatter point is sized by the significant wave height (m) and colored by the total distance from the shore (m).

Additionally, a correlation between wind speed and number concentration can be seen from observing the cumulative number concentration by bins (Figure 13). Higher wind speeds appear to be correlated to larger SSA concentrations and overall larger SSA sizes. It is visible, however, that samples with smaller wind speeds can reach cumulative number concentrations similar to those with higher wind speeds.

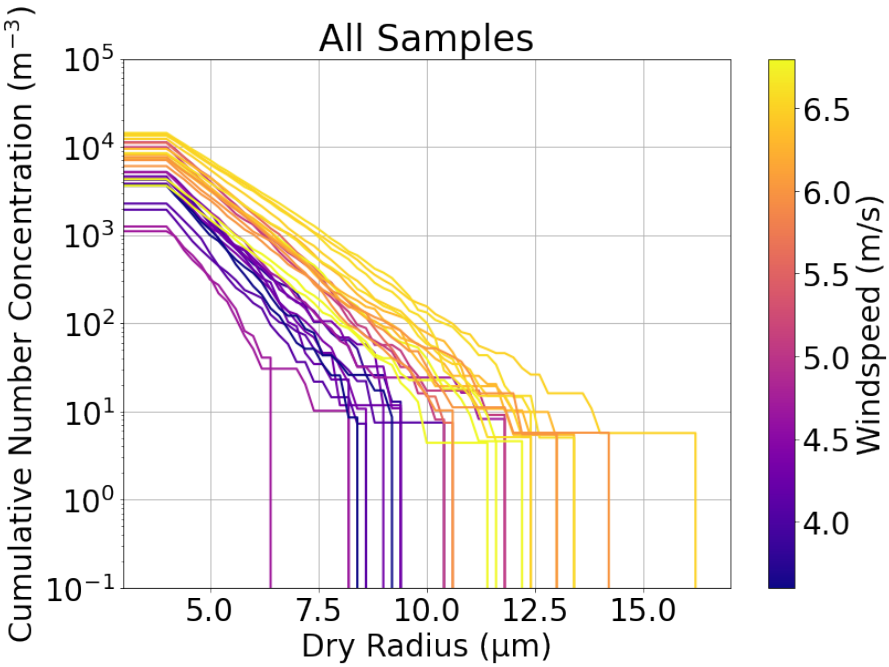

Figure 13. The cumulative number concentration (m^{-3}) of SSA on a log scale is plotted against the dry radius bins (µm) of the size distribution. Each line represents a different sample and is colored by the mean wind speed (m/s) of the sample.

Analysis at each sampling location was then necessary to determine how surface winds influenced concentrations in these regions (Figure 14). Shore samples were not used in this analysis because they were taken on the same day and therefore saw a very minimal change in

wind speeds. Number concentrations and total SSA mass are both weakly positively correlated to wind speeds in ocean samples. In both reef and lagoon samples, concentrations appear to be highly correlated to wind speeds (r^2>0.86), and total mass appears to have a slightly stronger correlation to higher wind speeds (r^2>0.94).

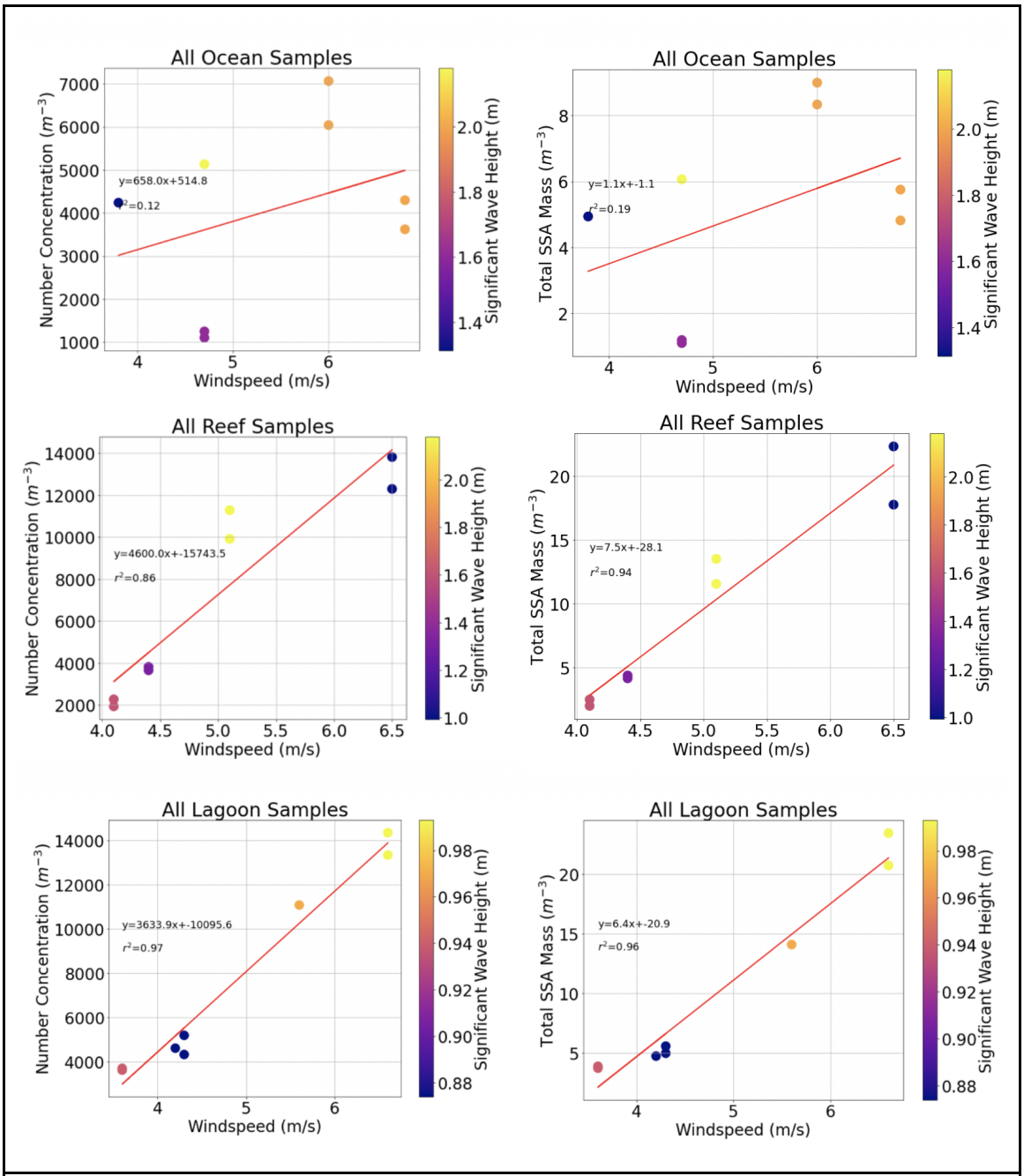

Figure 14. The total number concentration (left, m^{-3}) and total mass concentration (right, $\mu g/m^3$) are plotted against surface wind speed (m/s) for ocean (top), reef (middle), and lagoon (bottom) samples. Each scatter point is sized by the significant wave height (m) and colored by the total distance from the shore (m).

3.3 Significant Wave Height

The lagoon and shore samples were assigned to the grid box in the PacIOOS model closest to the coast, represented by the blue box within the black oval, while the fringing reef and open ocean samples were assigned to the red box within the black oval (Figure 15). The corresponding grid boxes were determined using their mean distance values from the shoreline. The modeled significant wave heights were then plotted against the total concentrations.

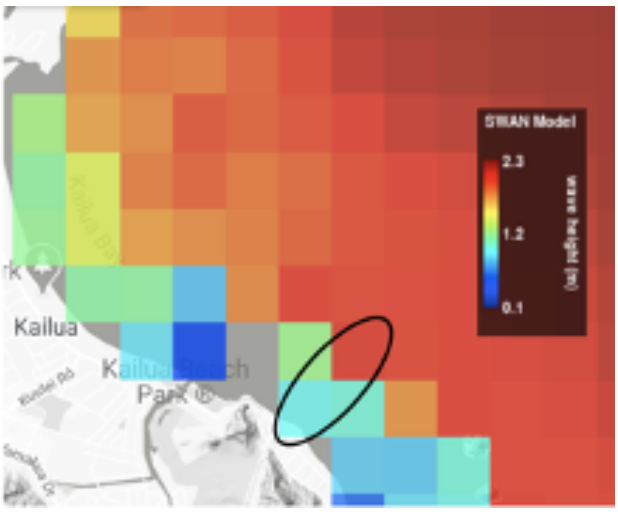

Figure 15. An example image of significant wave height (color, m) from the PacIOOS model near Lanikai beach for 191004. The circled black region represents the two grid points used for significant wave height in this analysis.

An overall negative correlation exists for significant wave height vs. concentrations. This could be potentially from wave attenuation at the fringing reef, causing smaller wave heights within the lagoon and shore region, while the fringing reef and open ocean concentrations are represented by wave heights unaffected by this bathymetry. Further investigation is needed to confirm this relationship.

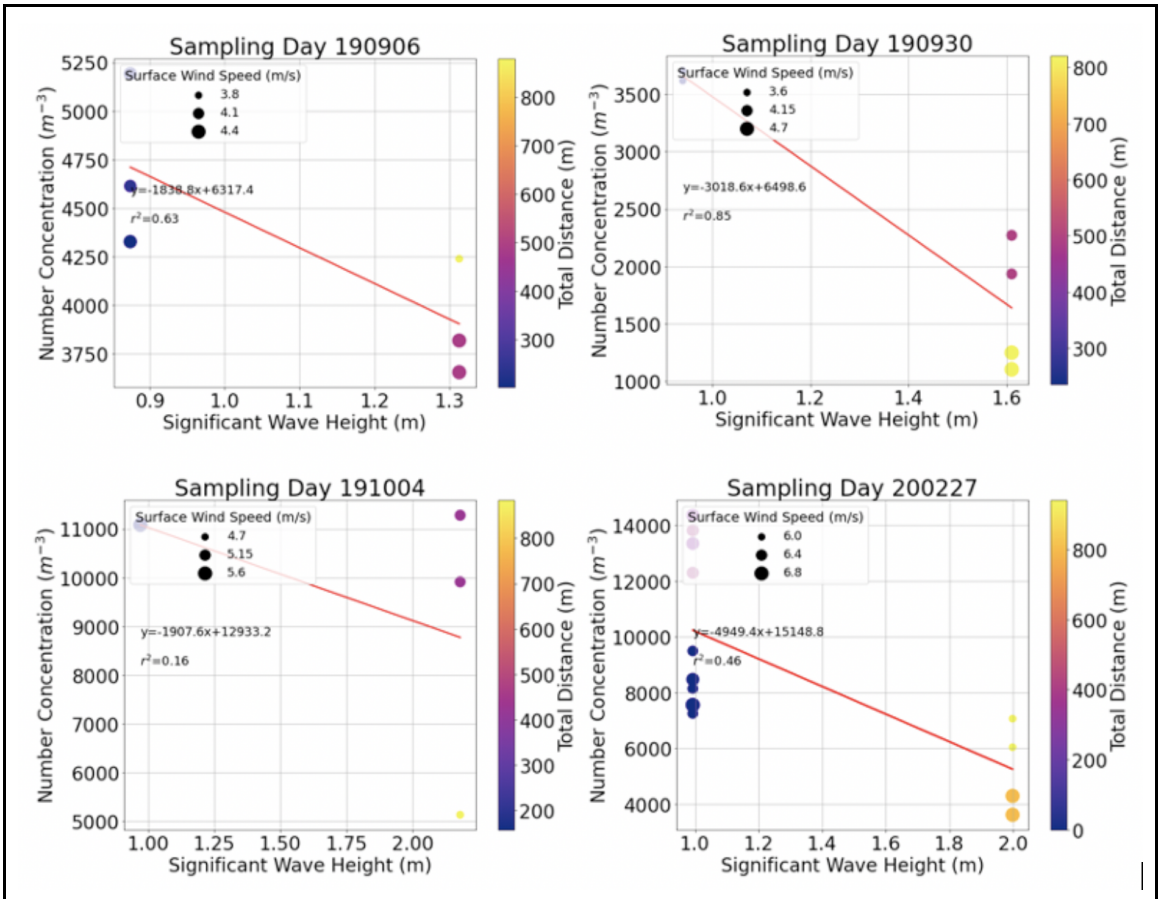

Figure 16. The total number concentrations (m^{-3}) are plotted against significant wave height (m) for four sampling days; 190906 (top left), 190930 (top right), 191004 (bottom left), and 200227 (bottom right). Each scatter point is sized by the surface wind speed (m/s) and colored by the total distance from the shore (m).

Chapter 4: Conclusions

This study assessed how distance from shore, wind speed, and modeled significant wave height contributed to SSA production across four sampling locations (open ocean, reef, lagoon, shoreline) and various sampling days. Preliminary analysis of SSA production within the surf zone demonstrates there are observable changes with distance from the coast. Several days showed relationships with a strong correlation (r^2>0.83) between SSA number concentration and total mass with distance offshore; however, variability occurs within this relationship which may imply that other coastal or temporal variables are important.

Normalizing the sample values showed that concentrations predominantly decreased with distance from the shore as well, highlighting their magnitude. In some cases, concentrations almost tripled the background concentration for that day, while other days saw smaller increases. Normalizing the total mass yielded similar results to the normalized concentrations, with two samples more than tripling their original background concentrations. Overall, both demonstrated increases in SSA with respect to the background across all locations except for two samples relative to open ocean concentrations. Further sampling needs to be conducted in order to properly assess this relationship and understand its robustness.

Additionally, a moderate relationship exists between surface wind speeds and observed SSA. An increase in wind speeds accounted for 40% of total concentration variance, and 47% of total mass variance. At specific sampling locations, the fringing reef and lagoon samples had the highest correlation to wind speeds (r^2>0.86), while the open-ocean concentrations had the weakest correlation to wind speeds for concentrations and total mass (r^2 > .019). The shore samples could not be compared to wind speed as they were all sampled on the same day within a small range of wind speeds.

Significant wave height also demonstrated some moderate correlations in three of the four sampling days ($0.86 > r^2 > 0.46$). The PacIOOS model provided insight into how significant wave height changed over the coastal bathymetry, proving useful in analysis against SSA change with distance from shore. Future analysis should be conducted with higher resolution coastal models in an attempt to gain more specific insights on wave activity from the shore.

In conclusion, this study has shown preliminary evidence for coastal contributions to SSA production. While considerable sampling is still necessary to confirm these relationships, and further analysis is needed to understand why, this study has provided evidence that change is indeed occurring. Additionally, analysis against other coastal variables, like wave steepness, wave speed, sea surface temperature, and others, should be analyzed in the future for potential relationships.

Chapter 5: References

Andreas, E. L (2002), A review of the sea spray generation function for the open ocean, in Atmosphere-Ocean Interactions, vol. 1, edited by W. Perrie, pp. 1–46, WIT, Southampton, U. K.

Anguelova, M. D. (2002). Sea Salt Aerosols. In *White Caps, Sea Salt Aerosol, and Climate* (pp. 7–22). Newark, DE: University of Delaware.

Garza, J. A., Chu, P.-S., Norton, C. W., & Schroeder, T. A. (2012). Changes of the prevailing trade winds over the islands of Hawai`i and the North Pacific. *Journal of Geophysical Research*.

Grythe, H., Ström, J., Krejci, R., Quinn, P., & Stohl, A. (2014). A review of sea-spray aerosol source functions using a large global set of sea salt aerosol concentration measurements. *Atmospheric Chemistry and Physics*, *14*(3), 1277–1297. https://doi.org/10.5194/acp-14-1277-2014

Hsu, N. C. (n.d.). How Aerosols Are Measured: The Science of Deep Blue. Retrieved December 10, 2019, from https://deepblue.gsfc.nasa.gov/science.

Jaeglé, L., Quinn, P. K., Bates, T. S., Alexander, B., & Lin, J. T. (2011). Global distribution of sea salt aerosols: New constraints from in situ and remote sensing observations. *Atmospheric Chemistry and Physics*, *11*(7), 3137–3157. https://doi.org/10.5194/acp-11-3137-2011

Jensen, J., & Nugent, A. (2017). Condensational growth of drops formed on giant sea-salt aerosol particles. *Journal of Atmospheric Sciences*, 679-697.

Kestrel 5 Series Weather/Environmental Meters. (2020, January 10). Retrieved from Kestrel Instruments: www.kestrelinstruments.com

Lewis & Schwartz. (2004). *Sea Salt Aerosol Production: Mechanisms, Methods, Measurements and Models•A Critical Review*.

Lowenthal, D., & Kumar, N. (2012). Light Scattering from Sea-Salt Aerosols at Interagency Monitoring for Protected Visual Environments (IMPROVE) Sites. *Journal of the Air & Waste Management Association*, 636-642.

McInnes, L., Bergin, M., Ogren, J., & Schwartz, S. (1998). Apportionment of light scattering and hygroscopic growth to aerosol composition. *Geophysical Research Letters*, 513-516.

Twomey, S. (December 1974). "Pollution and the planetary albedo". *Atmos. Environ*. **8** (12): 1251–6. Bibcode:1974AtmEn...8.1251T. doi:10.1016/0004-6981(74)90004-3

Vitousek, S., & Fletcher, C. H. (2008). Maximum Annually Recurring Wave Heights in Hawai'i. . *Pacific Science*, 541-555.